Free Radical Biology and Medicine 150 (2020) 40–52

Contents lists available at ScienceDirect

Free Radical Biology and Medicine

journal homepage: www.elsevier.com/locate/freeradbiomed

Original article

Free radicals derived from γ-radiolysis of water and AAPH thermolysis mediate oxidative crosslinking of eGFP involving Tyr-Tyr and Tyr-Cys bonds: the fluorescence of the protein is conserved only towards peroxyl radicals

Ricardo A. Zamora[a,1], Eduardo Fuentes-Lemus[a,1], Pablo Barrias[a], Alejandra Herrera-Morande[a,b], Francisco Mura[a], Victoria Guixé[b], Victor Castro-Fernandez[b], Tomás Rojas[a], Camilo López-Alarcón[c], Paulina Aguirre[d], Andrea Rivas-Aravena[e,**], Alexis Aspée[a,*]

[a] Departamento de Ciencias del Ambiente, Facultad de Química y Biología, Universidad de Santiago de Chile, Casilla 40 Correo 33, Santiago, Chile
[b] Departamento de Biología, Facultad de Ciencias, Universidad de Chile, Santiago, Chile
[c] Departamento de Química Física, Facultad de Química y de Farmacia, Pontificia Universidad Católica de Chile, Santiago, Chile
[d] Comisión Chilena de Energía Nuclear, Departamento de Tecnología Nucleares, Nueva Bilbao 12501, Santiago, 7600713, Chile
[e] Facultad de Medicina y Ciencia, Universidad San Sebastián, Lota 2465, Providencia, Santiago, 7510157, Chile

ARTICLE INFO

Keywords:
eGFP
Fluorescent proteins
Protein cross-linking
Cysteine-tyrosine bonds
di-tyrosine bonds

ABSTRACT

The enhanced green fluorescent protein (eGFP) is one of the most employed variants of fluorescent proteins. Nonetheless little is known about the oxidative modifications that this protein can undergo in the cellular milieu. The present work explored the consequences of the exposure of eGFP to free radicals derived from γ-radiolysis of water, and AAPH thermolysis. Results demonstrated that protein crosslinking was the major pathway of modification of eGFP towards these oxidants. As evidenced by HPLC-FLD and UPLC-MS, eGFP crosslinking would occur as consequence of a mixture of pathways including the recombination of two protein radicals, as well as secondary reactions between nucleophilic residues (e.g. lysine, Lys) with protein carbonyls. The first mechanism was supported by detection of dityrosine and cysteine-tyrosine bonds, whilst evidence of formation of protein carbonyls, along with Lys consumption, would suggest the formation and participation of Schiff bases in the crosslinking process. Despite of the degree of oxidative modifications elicited by peroxyl radicals ($ROO^{\bullet}$) generated from the thermolysis of AAPH, and free radicals generated from γ-radiolysis of water, that were evidenced at amino acidic level, only the highest dose of γ-irradiation (10 kGy) triggered significant changes in the secondary structure of eGFP. These results were accompanied by the complete loss of fluorescence arising from the chromophore unit of eGFP in γ-irradiation-treated samples, whereas it was conserved in $ROO^{\bullet}$-treated samples. These data have potential biological significance, as this fluorescent protein is widely employed to study interactions between cytosolic proteins; consequently, the formation of fluorescent eGFP dimers could act as artifacts in such experiments.

1. Introduction

The enhanced green fluorescent protein (eGFP) is one of the most employed engineered variants of the GFP-like protein family to investigate gene expressions and protein localization in living systems [1–4]. The widespread use of eGFP as fluorescent tag is supported by particular photophysical properties of its chromophore which are maintained in intra- and extra-cellular milieus [5,6]. The latter, which is shared with related fluorescent proteins, is conferred by the structural stability of their tertiary structure, where the chromophore is located inside of a beta barrel [7,8].

The popularity of eGFP is partially explained by the fact that visualization of its chromophore is non-invasive, requiring only irradiation with blue light of cell cultures or other biological systems [9,10]. It

* Corresponding author.
** Corresponding author.
E-mail addresses: andreara@gmail.com (A. Rivas-Aravena), alexis.aspee@usach.cl (A. Aspée).
[1] Both Authors contributed equally to this work.

https://doi.org/10.1016/j.freeradbiomed.2020.02.006
Received 30 December 2019; Received in revised form 29 January 2020; Accepted 8 February 2020
Available online 17 February 2020

should be noted that the sturdiness of the photophysical properties of the chromophore is such, that even under conditions favoring non-covalent eGFP oligomerization, the fluorescence spectrum is red-shifted only in 2 nm [11]. However, in spite of this, dimerization and oligomerization of eGFP, together with formation of adducts with cellular proteins, could interfere with the experimental measurements aimed to explore interactions between cytosolic proteins [12,13]. Thus, to avoid eGFP oligomerization, experimental conditions, as well as the design of the linker between the tag (eGFP) and the protein under study should be carefully monitored and planned [14].

It has been reported that maturation of the eGFP chromophore occurs inside the beta barrel after cyclization and dehydration processes involving the residues Ser65, Tyr66 and Gly67 (Supplementary Fig. 1) [15]. In the presence of O_2, this is followed by an autocatalytic oxidation leading to the formation of superoxide ($O_2^{\bullet-}$) and hydrogen peroxide (H_2O_2) [15,16]. Such production of reactive oxygen species, which are able to induce damage on biological environments, has been denoted as a shortcoming of using eGFP as a fluorescent tool [15,17]. In fact, in the presence of NADH, production of H_2O_2 at a rate of 0.4 μM/min has been determined, reaching after 8 h incubation a total H_2O_2 concentration close to nineteen times higher than the total eGFP concentration [15].

It is well-known that living cells possess enzymatic (protective) systems to deal with $O_2^{\bullet-}$ [18]. These pathways mediate $O_2^{\bullet-}$ dismutation to O_2 and H_2O_2, and the catalytic conversion of H_2O_2 to H_2O and O_2 [18]. Nonetheless, accumulation of H_2O_2 during eGFP maturation would overcome the protective system inducing oxidative reactions. In particular, inside the cytosol, H_2O_2 (half-life $\approx 10^{-3}$ s) could mediate Fenton-like reactions in the presence of low-valence transition metals such as iron or copper, generating hydroxyl radical ($^{\bullet}OH$) [19,20]. In comparison with H_2O_2 and $O_2^{\bullet-}$, the reactivity of $^{\bullet}OH$ ($E^{\circ} = 2.3$ V [21], half-life $\approx 10^{-9}$ s) is significantly higher, explaining its fast and non-selective reactions towards biomolecules [19]. In addition to the potential exposure of eGFP to reactive species derived from its chromophore maturation, in biological systems, eGFP could also be exposed to the reactive species produced as consequence of cellular metabolism, such as $^{\bullet}OH$, $O_2^{\bullet-}$, H_2O_2, and peroxyl radicals ($ROO^{\bullet}$). The latter are produced during peroxidation of membrane lipids [22].

As mentioned above, the particular structural conformation of eGFP gives to this protein a high structural stability inside cells [8]. Notwithstanding this, eGFP can be a target of oxidants, inducing modifications on the side chain of amino acids and potentially in the structure of its chromophoric unit. This due to reactive oxygen species that rapidly react with the side chain of exposed residues, highlighting those present in tryptophan (Trp), tyrosine (Tyr), methionine (Met), histidine (His), and cysteine (Cys) [22,23]. The first step of the oxidation of these amino acids leads to the formation of secondary free radicals whose self-reactions generate covalent bonds. Particularly, Tyr-derived phenoxyl ($Tyr^{\bullet}$) and Cys-derived thiyl radicals ($Cys^{\bullet}$), produce diTyr and disulphide bonds, respectively, two recognized covalent adducts that mediate intra- or inter-protein cross-linking [22]. Furthermore, there is evidence showing production of tryptophanyl radicals ($Trp^{\bullet}$) and their participation in diTrp bonds leading to intra- or intermolecular protein cross-linking [24,25]. In addition to these reaction pathways of protein cross-linking (through radical-radical reactions), the formation of carbonyl groups owing to amino acid oxidation, and their reaction with nucleophilic side chains of some residues (e.g. Cys, Lys or Arg), could also lead to protein cross-linking through formation of Schiff bases [22,23].

In spite of the well-known production of reactive species in cells, and the recent findings showing that oxidants are also produced during eGFP maturation, it has not been investigated how oxidative reactions could affect eGFP structure and its fluorescent properties that are key for its use as biomolecular tool. Taking into account the structural properties of eGFP, we hypothesize that its exposure to free radicals derived from the γ-radiolysis of water, and the thermolysis of 2,2′-azobis (2-methylpropionamide) dihydrochloride (AAPH) would induce the oxidation of susceptible residues leading to the generation of secondary free radicals that can mediate eGFP cross-linking affecting its fluorescence. Aimed to test such hypothesis, experiments to elucidate the oxidative changes on the molecular mass of eGFP were carried out. SDS-PAGE analysis, extent of amino acid consumption, quantification of oxidation products, circular dichroism (CD), fluorescence, size exclusion chromatography, and mass spectrometry analysis, were employed with such goal.

2. Materials and methods

2.1. Reagents

2,2′-azobis (2-methylpropionamide) dihydrochloride (AAPH), 3,4-dihydroxyphenylalanine (DOPA), DL-kynurenine (Ky), sodium dodecyl sulfate (SDS), methanesulfonic acid (MSA, 4 M) containing tryptamine (0.2% w/v), trichloroacetic acid (TCA), *o*-phthaldialdehyde (OPA), β-mercaptoethanol, 2,4-dinitrophenylhydrazine (DNPH), methionine sulfoxide (MetSO), amino acids standard solution, and the reagents employed for SDS-PAGE analysis were purchased from Sigma-Aldrich (St Louis, MO). Di-Tyrosine (diTyr) and N-formylkynurenine (NFKy) were obtained from Toronto Research Chemicals (Toronto, CA). Sodium perchlorate was purchased from Merck KGaA (Darmstadt, Germany). All solvents employed were HPLC grade.

2.2. Expression and purification of eGFP

eGFP sequence was amplified by PCR from pEGFP-N1 vector (Clontech). The primers used were Fw: 5′GGAATTCCATATGGTGAGC AAGGG3′ and Rev: 5′ CGCGGATCCTTACTTGTACAGCTCG3′, which contain restrictions site for *Nde*I and *Bam*HI, respectively. The amplified product was cut with *Nde*I/*Bam*HI and cloned into the modified pET-28b vector, which inserted a N-terminal hexahistidine tag joined to a TEV protease recognition site. *E. coli* strain BL21 (DE3) was transformed with modified pET-28b-eGFP vector for protein expression. Cells were cultured at 37 °C in LB broth containing 35 mg mL^{-1} kanamycin and grown until OD_{600} of 0.8. Protein expression was induced by adding 1 mM of isopropyl-b-D-thiogalactopyranoside (IPTG) and cultures were incubated at 25 °C overnight. Bacterial cells were harvested by centrifugation at 7000 rpm for 10 min at 4 °C. The bacterial pellet was resuspended in 50 mL of binding buffer (50 mM Tris-HCl pH 7.8, 30 mM Imidazole, 500 mM NaCl, 1 mM PMSF, 1 mM DTT and 5% glycerol) and disrupted by sonication. The suspension was centrifuged at 12,000 rpm for 30 min at 4 °C. The soluble fraction was loaded onto a Ni^{+2}-sepharose affinity column (HisTrap HP, GE Healthcare, UK) pre-equilibrated with binding buffer. The column was washed with 50 mL of binding buffer and eluted with a linear gradient of imidazole between 30 and 500 mM. The fraction containing a green fluorescent protein were pooled and dialyzed against 75 mM sodium phosphate buffer pH 7.4. The dialyzed volume was loaded onto a molecular exclusion column (Superdex 75 16/60, GE Healthcare, UK). This purification step confirmed that eGFP was in its monomeric form (Supplementary Fig. 2). The purity of the protein was confirmed by SDS-PAGE stained with Coomassie Brilliant Blue (Data not shown). Protein concentration was determined by measuring the absorbance at 280 nm and 490 nm and employing an extinction coefficient of 13,410 M^{-1} cm^{-1} and 56,000 M^{-1} cm^{-1}, respectively [1]. The spectral properties of pure eGFP samples showed to be similar to those reported in literature, with a λ_{ex} of 490, and λ_{em} of 507 nm (Supplementary Fig. 2) [1].

2.3. Protein oxidation

Experiments aimed to study eGFP oxidation mediated by free radicals generated from the thermolysis of AAPH and the γ-radiolysis of

water were performed 48 h after the expression and purification of the protein to ensure the complete maturation of the chromophore. Working solutions containing eGFP at 66 μM (2 mg mL^{-1}) and AAPH (30 or 100 mM, final concentration) were prepared in phosphate buffer 75 mM, pH 7.4. Solutions were incubated at 37 °C for 120 min. Aliquots were taken after 15, 30, 45, 60, 90 and 120 min of reaction, cooled to 4 °C and dialyzed (at 4 °C). Dialyzed solutions, not containing AAPH, were stored at −80 °C until analysis. Control solutions (eGFP without AAPH) were incubated and analyzed employing the same procedures that working solutions. For steady-state irradiation, aerated samples containing eGFP (2 mg mL^{-1}) in phosphate buffer solution (75 mM) pH 7.4 were inserted into the chamber of a Gamma 3500 Noratom (Horton, Norway) instrument that employs ^{60}Co as γ-radiation source. The dose of γ-radiation was determined employing the ferrous sulfate dosimeter system [26,27], and irradiation of samples was performed until a cumulative dose of 2 or 10 kGy was achieved after 221 and 1102 min, respectively. After oxidation, samples were aliquoted and stored at −80 °C until analysis.

2.4. SDS-PAGE analysis

Changes in the molecular mass of eGFP were examined by SDS–PAGE electrophoresis under reducing and non-reducing conditions. Aliquots of control or oxidized samples (75 μL) were mixed with 25 μL of loading buffer composed of Tris buffer (62.5 mM, pH 6.8), SDS (2% v/w), glycerol (10% v/v), and traces of bromophenol blue as a tracking dye for non-reducing SDS-PAGE experiments. For reducing SDS-PAGE analysis it was employed the same loading buffer but containing β-mercaptoethanol (100 mM). Once mixed with the corresponding loading buffer, samples were incubated for 5 min at 90 °C. Acrylamide (4%) stacking gel, 12% acrylamide resolving gels, and a running buffer comprising Tris (25 mM), Gly (400 mM), and SDS (1% w/v) were used. Electrophoresis was performed at 120 V for 120 min. After electrophoresis, gels were stained with colloidal Coomassie.

2.5. Monomer consumption

Aliquots (30 μL) of control and oxidized samples of eGFP were diluted 20-fold in a solution containing sodium phosphate (50 mM), sodium chloride (150 mM), SDS 1% (w/v) and DL-dithiothreitol (50 mM). These solutions were then heated to 90 °C during 10 min to denature the proteins. Denatured samples were transferred to HPLC vials and separated using an Agilent 1200 series HPLC, equipped with a Multisampler Agilent 1260 series Infinity II (set at 20 °C) and a diode array detector (Agilent 1200 series). Chromatographic separation was achieved using a flow rate of 0.8 mL min^{-1} by size exclusion chromatography employing a BioSep™ SEC-s3000 (5 μm, 290 Å, 300 × 7.8 mm, Phenomenex, Torrance, CA, USA) column kept at 40 °C. Separation was achieved using a binary gradient of mobile phases A (ultrapure water containing 0.1% TFA) and B (acetonitrile containing 0.1% TFA). The gradient elution program was the following: 0 min 35% B, 0–25 min increase B to 50%, 25–26 min return to 35% B, 26–35 min 35% B. Absorbance was monitored at 220 nm. Data analysis was carried out using OpenLAB (Santa Clara, CA, USA) software.

2.6. Analysis of amino acid consumption by HPLC with pre-column derivatization and fluorescence detection

Control and oxidized samples of eGFP were hydrolyzed to free amino acids according to the methodology described by Hawkins and coworkers [28]. 200 μL of the reaction mixtures were transferred to glass hydrolysis vials and samples were precipitated by adding 50 μL of 50% w/v aqueous solution of TCA. Samples were centrifuged at 9000 g at 4 °C. The obtained protein pellets were washed twice with cold acetone and dried using a stream of nitrogen gas. Pellets were resuspended in 150 μL of 4 M MSA containing 0.2% w/v tryptamine. O_2 was removed using repeated vacuum treatment and N_2 gassing, closing the vials under vacuum before transferring them into an oven kept at 110 °C to perform hydrolysis overnight employing a Pico-Tag system. After cooling, the samples were neutralized with 4 M NaOH, filtered through 0.2 μm Pall Nanosep filters and diluted 20-fold with water. Diluted samples (30 μL) were transferred to HPLC vials and separated by HPLC using an Agilent 1200 series system equipped with an Agilent 1260 series auto sampler (with the samples kept at 4 °C) and an Agilent 1260 series fluorescence detector. Samples were derivatized by adding 10 μL of an activated OPA solution and incubated for 1 min, immediately before injection (4 μL) on to a reversed phase column (Hibar® 250 × 4.3 mm RP-18 endcapped (particle size 5 μm) Phurospher® STAR, Millipore, maintained at 40 °C). Samples were eluted using a gradient of buffer A (100 mM sodium acetate pH 5.3, 2.5% tetrahydrofuran, 20% methanol in water) and B (100 mM sodium acetate pH 5.3, 2.5% tetrahydrofuran, 80% methanol in water), at a flow rate of 0.8 mL min^{-1} as described by Leinisch et al. [29]. Fluorescence was monitored employing λ_{ex} = 340 nm, λ_{em} = 440 nm. Data analysis was carried out using OpenLab Software (Santa Clara, CA). To identify and quantify eluting species, standards of amino acids were run under identical conditions, and, calibration curves were constructed from which the amino acid concentrations of samples were determined. To minimize concentration variations arising during the protein hydrolysis, the data were normalized to the concentration of Leu residues.

2.7. Quantification of oxidation products of Tyr and Trp

Protein samples were hydrolyzed (with MSA) and neutralized with 4 M NaOH, filtered through 0.2 μm Pall Nanosep filters and diluted 10-fold with water (as described above), then the oxidation products of Trp (NFKy, Ky) and Tyr (DOPA and diTyr) were analyzed as previously described [25,28]. Under the acidic conditions employed, NFKy is hydrolyzed to Ky, thus these data are reported as the sum of these species (NFKy + Ky) [29]. Samples (20 μL) were injected onto a reverse phase column Hibar® 250 × 4.3 mm RP-18 endcapped (particle size 5 μm, Phurospher® STAR, Millipore) maintained at 30 °C, and separated by gradient elution using buffer A (100 mM sodium perchlorate, 10 mM, H_3PO_4) and buffer B (80% aqueous methanol), at a flow rate of 0.8 mL min^{-1}. Oxidation products were monitored setting the DAD detector at 260, 280, 310 and 370 nm, and the fluorescence detector at a single λ_{ex}: 280 nm with multiple λ_{em}: 320, 350, 410 and 510 nm for detection. Data analysis was carried out using OpenLab Software (Santa Clara, CA). Identification of specific species was determined by comparison to the authentic commercial standards, which were also used to construct standard curves and determine the concentrations of the products.

2.8. Quantification of total protein carbonyls

Sample preparation and quantification of protein carbonyls in oxidized samples was done according to the methodology described by Hawkins and co-workers [28]. Briefly, 200 μL of DNPH solution (10 mM in HCl 2.5 M) were added to aliquots (200 μL) of control and oxidized protein samples and incubated in dark at room temperature for 15 min. Afterwards, derivatized proteins were precipitated by adding 100 μL of TCA 50% (w/v) to each tube (final TCA concentration of 10% w/v). Samples were then incubated at −20 °C during 20 min before centrifuging at 9000g for 15 min at 4 °C. The supernatant was discarded without disturbing the protein pellet. Then the pellet was washed two times with ice-cold ethanol and ethyl acetate (1:1 mixture solution) with centrifugation steps (2 min at 9000g) between washes. Protein pellets were dissolved in a 6 M guanidine-HCl solution. Finally, the absorbance of the DNP-derivatized samples was recorded at 370 nm using a Synergy HTX multi-mode microplate reader (BioTek Instruments, Winooski, VT, USA). Total protein carbonyl concentration was determined using the extinction coefficient of DNP at 370 nm

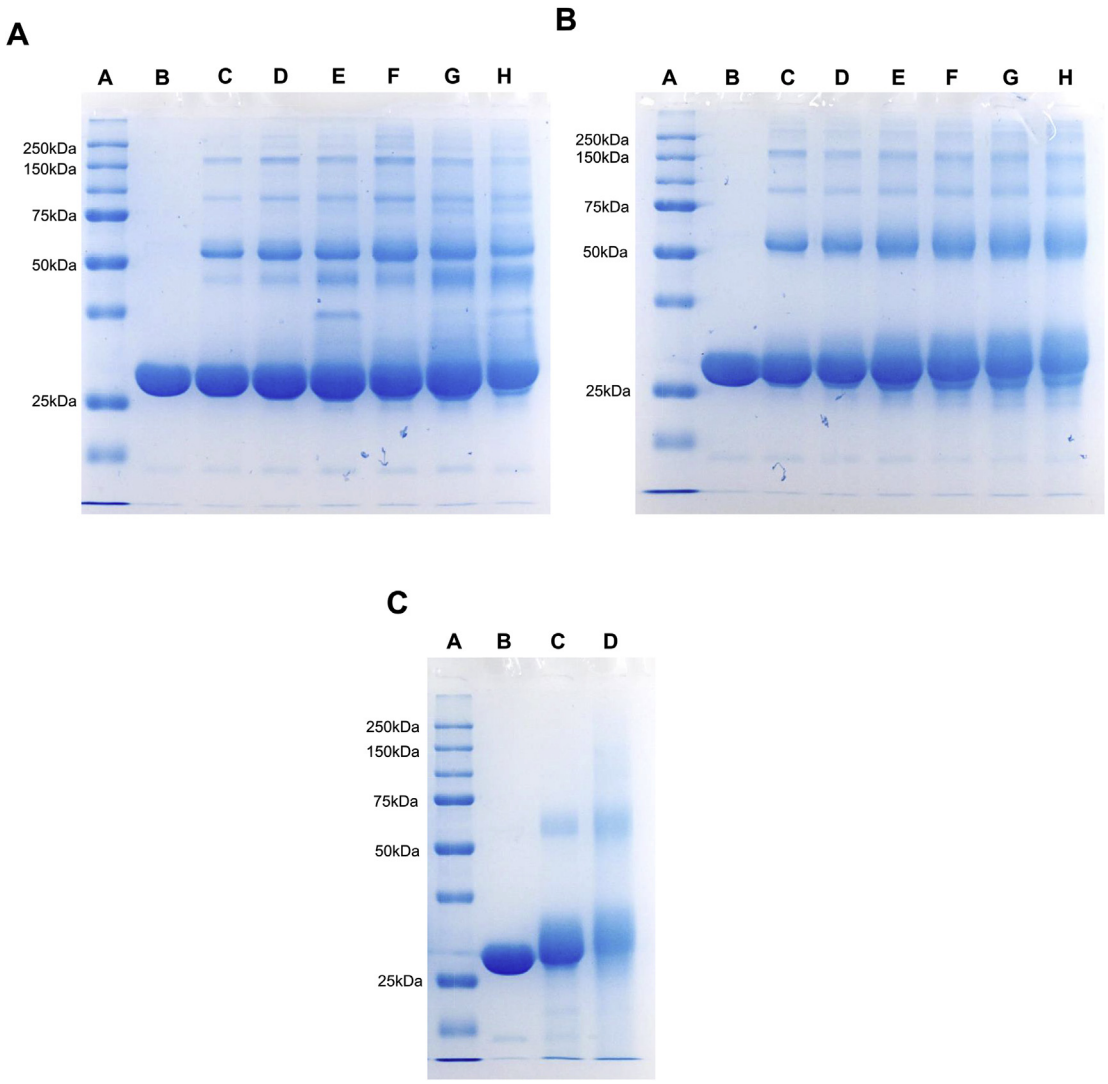

Fig. 1. SDS-PAGE analysis of the changes in the apparent molecular mass of eGFP after its exposure to AAPH- or γ-irradiation-derived free radicals in phosphate buffer (75 mM, pH 7.4). Samples containing eGFP (2 mg mL^{-1}, 66 μM) were incubated at 37 °C with AAPH 30 (Panel A) or 100 mM (Panel B) during 2 h taking aliquots every 15 min or exposed to ^{60}Co γ-irradiation until a desired cumulative dose of 2 or 10 kGy was achieved (Panel C). Aliquots of control and oxidized samples were treated as described in the Materials and methods, prior to loading 22 μg of protein into each well of the gel. For Panel A and B: Lane A = molecular weight markers; Lane B = control. Lanes C–H = aliquots taken after 15, 30, 45, 60, 90 and 120 min. For Panel C: Lane A = molecular weight markers; Lane B = control; Lane C = cumulative dose of 2 kGy; and Lane D = cumulative dose of 10 kGy.

($22{,}000\ M^{-1}\ cm^{-1}$) [28].

2.9. Mass spectrometric analysis of oxidation products

Hydrolyzed protein samples were analyzed employing an ultra-high performance liquid chromatography UPLC Ultimate 3000 RSLC system coupled to a Linear Ion Trap Mass Spectrometer LTQ XL (Thermo scientific). A Hibar® 250 × 4.3 mm RP-18 endcapped (particle size 5 μm, Phurospher® STAR, Millipore) column was used as stationary phase and maintained at 30 °C. Gradient elution with buffer A (formic acid 0.1%) and buffer B (50/50 water/methanol mixture containing 0.1% of formic acid) at a rate of 0.2 mL min^{-1} was employed as mobile phase. Buffer B was kept at 0% for the first 1 min before increasing to 80% over 18 min. Then, buffer B was kept constant at 80% during 10 min before decreasing back to 0% over 3 min. Finally, the system was equilibrated with 0% B for 9 min. Mass detection was carried out using electrospray ionization (ESI), with the spray voltage set at 3 kV (at 350 °C). Detection was performed in full scan mode in the 100–800 *m/z* range in positive mode. MS2 spectra were obtained using He for collision-induced fragmentation (CID) with a normalized collision energy of 35 units and detection of fragments in full scan mode as previously described [25,30].

2.10. Analysis of the changes in the secondary structure of eGFP as consequence of its oxidation

Control and oxidized samples of eGFP were analyzed by circular dichroism (CD). Far-ultraviolet CD spectra were recorded on a Jasco J-1500 spectropolarimeter (Jasco, Easton, MD) using a 1 mm cuvette cell. Before analysis, each sample was diluted to a concentration of 0.2 mg mL^{-1} in sodium phosphate buffer 75 mM, pH 7.4. The collected spectra correspond to the average of 4 scans realized between 190 nm and 250 nm (with 1 nm bandwidth) at 25 °C, 4 s of D.I.T., 0.2 nm of data pitch and a speed of 50 nm min^{-1} in a continuous mode.

2.11. Analysis of the fluorescence arising from the soluble protein aggregates generated upon eGFP oxidation

After oxidation, samples were centrifuged at 22,000g. Supernatant was loaded onto a molecular exclusion column (Superdex 75 16/60, GE

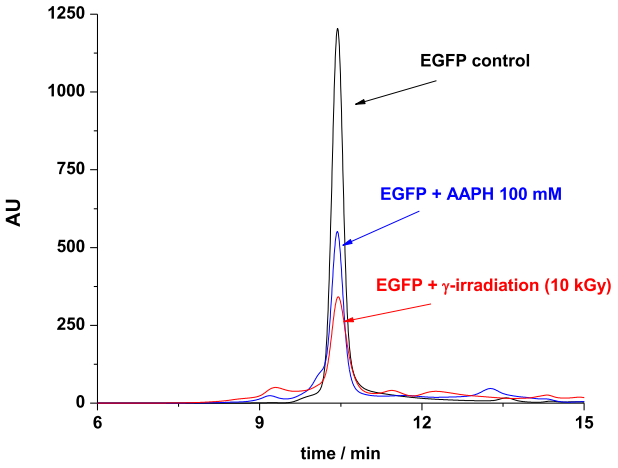

Fig. 2. Determination of the consumption of the monomeric eGFP after exposure of protein samples to ROO$^{\bullet}$ or ^{60}Co γ-irradiation by HPLC with diode array detection. Aliquots (30 μL) of control or oxidized samples of eGFP (66 μM) were injected into an HPLC system and separated employing a Phenomenex® BioSep™ 5 μm SEC-s3000 290 Å (300 × 7.8 mm) column as described in materials and methods section. The monomeric band was followed at 220 nm. Black line correspond to the control whereas blue and red lines correspond to samples of eGFP incubated at 37 °C with AAPH (100 mM) during 2 h and exposed to ^{60}Co γ-irradiation until a cumulative dose of 10 kGy was achieved, respectively. (For interpretation of the references to colour in this figure legend, the reader is referred to the Web version of this article.)

Healthcare, UK), which was pre equilibrated with the same buffer that contained the sample. The molecular exclusion column was connected to an HPLC with diode array detector. The absorbance of the sample was monitored at 220 nm and 280 nm. Upon injection into the HPLC system only two peaks corresponding to the oxidized monomeric and dimeric forms of eGFP were registered at 280 nm (Supplementary Fig. 3). Both the oxidized monomeric and dimeric forms of eGFP were individually collected, and the fluorescence spectrum of each one was registered employing a fluorimeter Jasco 8300 (Jasco, Easton, MD).

2.12. Statistical analysis

Data are presented as mean ± standard deviations from at least three independent experiments. Statistical analysis were carried out employing a one-way Anova with Turkey's post-hoc test, available in the software Microcal Origin® 8.

3. Results

3.1. Changes in the molecular mass of eGFP mediated by AAPH-derived ROO$^{\bullet}$ and γ-irradiation-generated free radicals

AAPH generates alkyl radicals (upon thermolysis), which rapidly react with O_2 ($k > 1 \times 10^9$ $M^{-1}s^{-1}$) producing ROO$^{\bullet}$ at a constant and known rate in the first hours of incubation [31]. To investigate the oxidative modifications on eGFP induced by ROO$^{\bullet}$, solutions containing eGFP (2 mg mL^{-1}; 66 μM) and AAPH (30 or 100 mM) were incubated at 37 °C. Aliquots were taken, dialyzed and analyzed by SDS-PAGE. As Fig. 1A and B depict, only one strong band was detected in the SDS-PAGE gels at cero incubation time in agreement with the molecular mass of eGFP (~30 kDa, including the poly-His Tag). Incubation with AAPH (30 or 100 mM) resulted in the consumption of the monomeric band, and the formation of crosslinked species. In fact, at different incubation times, dimers, trimers, and protein aggregates of molecular masses over 100 kDa were observed in samples incubated with AAPH 30 mM (Fig. 1A). Obtained results showed that eGFP cross-linked species were early generated (after 15 min of incubation), and the intensity of their bands increased until 75 min (Lane G, panel A) of incubation with AAPH 30 mM. Additional to these species, protein crosslinks with molecular masses between 30 and 50 kDa were detected (Fig. 1, **panel A**). Similar findings were evidenced when eGFP was incubated with AAPH 100 mM, however, the species with masses ranging between 30 and 50 kDa were not generated during the time of experiments (Fig. 1, **panel B**). To get more insights into the nature of the cross-links, SDS-PAGE analysis was carried out under non-reducing conditions (Supplementary Fig. 4). These results showed that cross-linked species ranging between 30 and 50 kDa evidenced in samples incubated with AAPH 30 mM are early generated (Supplementary Fig. 4). The pattern of formation of crosslinked species corresponding to dimers and higher molecular mass aggregates were similar than those evidenced under reducing conditions for both 30 and 100 mM AAPH-treated samples.

Aimed to compare the damage inflicted by ROO$^{\bullet}$ on eGFP with other oxidants that are generated inside the cell, samples containing eGFP (66 μM) were exposed to steady-state γ-irradiation from a ^{60}Co-source, which generates $^{\bullet}$OH, $O_2^{\bullet-}$, and H_2O_2 in aerated aqueous solutions [32,33]. Samples were irradiated during 221 or 1102 min until a cumulative dose of 2 and 10 kGy was achieved, respectively. The latter implies a total generation of 0.560 and 2.798 μmol of $^{\bullet}$OH in the system for the doses 2 and 10 kGy, respectively [33]. SDS-PAGE analysis of oxidized samples of eGFP mediated by free radicals generated from the γ-radiolysis of water exhibited a decrease of the monomeric band in a dose irradiation depending manner. Such decrease was accompanied by production of species with higher molecular mass than the eGFP monomer (Fig. 1, **Panel C**).

To quantify the amount of protein modified by AAPH and ^{60}Co γ-source, oxidized samples were studied by HPLC-DAD technique. Results, presented in Fig. 2, showed a single HPLC peak at 10.4 min attributed to the native eGFP monomer. After 2 h incubation with AAPH, a consumption of 26.1 and 31.9 μM of the monomeric eGFP was determined for AAPH 30 and 100 mM, respectively (Table 1 and Fig. 2). As crosslinked species are the major products of eGFP oxidation, it is possible to attribute the decrease of eGFP monomers as the amount of such species. That means that 39.6 and 48.2% of the original monomeric eGFP was involved in the formation of covalent oligomers in the presence of AAPH 30 and 100 mM, respectively. Similarly, exposure of eGFP samples to a ^{60}Co γ-source, induced a consumption of the monomer leading to a decrease of HPLC-DAD peak corresponding to 39.2 and 42 μM, for doses of 2 and 10 kGy, respectively (Table 1 and Fig. 2).

Table 1
Quantification of the remaining monomeric eGFP in control and oxidized samples mediated by AAPH- or γ-irradiation-derived free radicals. Samples containing eGFP (66 μM) were incubated with AAPH (30 or 100 mM) at 37 °C or exposed to ^{60}Co γ-irradiation until a desired cumulative dose of 2 or 10 kGy was achieved. Samples were then separated and analyzed by HPLC with diode array detector following the signal of the monomeric band at 220 nm. Results are presented as μM and percentage of the remaining monomer (in parenthesis). Values correspond to the mean ± standard deviation from at least three experiments.

Samples	Monomeric form, μM (%)
eGFP control	66 (100)
AAPH 30 mM	39.9 ± 0.8 (60.4)
	34.1 ± 3.9
AAPH 100 mM	(51.8)
2 kGy	26.8 ± 0.9 (40.5)
	24.0 ± 2.2
10 kGy	(36.3)

Table 2
Extent of amino acid consumption after exposure of eGFP to peroxyl radicals or hydroxyl radicals. Control and oxidized samples (AAPH- or ^{60}Co γ-irradiation-mediated) of eGFP (66 μM) were submitted to acidic hydrolysis as described in material and methods section prior to its analysis by HPLC employing the OPA-precolumn derivatization. Values are expressed as the concentration of consumed amino acid (μM), and as moles of consumed residues per mole of protein (in parenthesis). Values correspond to the mean ± standard deviation from at least three experiments.

	Met	His	Tyr	Lys
AAPH 30 mM	153.3 ± 11.9 (2.3)	0 (0)	44.5 ± 32.7 (0.7)	112.5 ± 59.7 (1.7)
AAPH 100 mM	256.1 ± 15.5 (3.9)	39.5 ± 21.3 (0.6)	104.1 ± 42.7 (1.6)	144.9 ± 76.0 (2.2)
2 kGy	99.1 ± 9.5 (1.5)	74.1 ± 16.6 (1.1)	23.7 ± 21.6 (0.3)	125.8 ± 40.4 (1.9)
10 kGy	172.4 ± 11.4 (2.6)	120.2 ± 19.1 (1.8)	19.1 ± 17.2 (0.3)	172.2 ± 13.7 (2.6)

3.2. Extent of amino acid consumption

Control and oxidized samples of eGFP were digested to amino acids through acidic hydrolysis and then analyzed by HPLC with fluorescence detection employing OPA pre-column derivatization [28]. The amino acid content of control samples was similar to that expected according to the primary structure of eGFP (Supplementary Figs. 5 and 6). Off the sixteen amino acids that can be quantified by this methodology only Tyr and Met showed a significant consumption in AAPH-incubated samples (Table 2). This result is in agreement with the selectivity of ROO$^{\bullet}$ which is explained by their reduction potential of E° = 1.0 V [21]. Due to chromatographic interferences, detection and quantification of the single Trp residue of eGFP was not possible by HPLC with OPA-precolumn derivatization [34,35]. Notwithstanding the aforementioned, detection and quantification of the oxidation products of Trp, which was possible employing other chromatographic methodologies, showed that Trp was partially modified by ROO$^{\bullet}$ and γ-radiation-generated free radicals (*vide infra*).

Table 2 depicts the extent of amino acid consumption (μM) triggered by AAPH and ^{60}Co γ-source. As the content of His and Lys could be directly or indirectly affected by the employed oxidant systems, both amino acids were also included in this table. Samples incubated with AAPH 30 mM presented a consumption of 153.3 and 44.5 μM of Met and Tyr, respectively. Considering a ROO$^{\bullet}$ production rate of 2.4 μM/min for AAPH 30 mM (at 37 °C) [31], after 2 h of incubation, a total dose of 288 μM of ROO$^{\bullet}$ was generated. These values indicate that Met was the prevalent target of ROO$^{\bullet}$ trapping close to 53% of the total amount of free radicals produced (Table 2). With AAPH 100 mM, similar results were found presenting a higher degree of oxidation of Met and Tyr. In addition, consumption of His was also evidenced. A consumption of 256.1, 104.1, and 39.5 μM of Met, Tyr, and His were evidenced, respectively (Table 2). After 2 h of incubation at 37 °C a total dose of 960 μM of ROO$^{\bullet}$ is generated from AAPH 100 mM. Taking into account these values, Met and Tyr showed to be the most reactive amino acids as they trapped 27 and 11% of the total ROO$^{\bullet}$ generated, respectively. Interestingly, Lys, an unreactive amino acid towards ROO$^{\bullet}$, was also consumed when eGFP was incubated with AAPH. A consumption of 112.5 and 144.9 μM of Lys were determined for samples incubated with AAPH 30 and 100 mM, respectively (Table 2).

For γ-irradiated samples only His, Met and Lys showed to be significantly consumed (Supplementary Fig. 6). For samples irradiated until a cumulative dose of 2 kGy 99.1, 74.1 and 125.8 μM of Met, His and Lys were consumed, respectively (Table 2). This implies that 0.299 μmol of amino acids were consumed under this condition. Considering that $^{\bullet}$OH is the most reactive specie amongst the generated from γ-radiolysis of water, and that 0.560 μmol of $^{\bullet}$OH would be generated for the dose of 2 kGy, 53.4% of the total amount of $^{\bullet}$OH were trapped by these 3 amino acids. A similar result was obtained for the eGFP samples oxidized with the highest dose of γ-radiation (10 kGy). Under this condition 172.4, 120.2, and 172.2 μM of Met, His and Lys were consumed giving a total amount of 0.465 μmol of consumed amino acids (Table 2). This value implies that these amino acids trapped only close to 17% of the total amount of $^{\bullet}$OH generated in the system. Remarkably, in spite of the high abundancy of Tyr residues in the primary structure of eGFP, this amino acid was not significantly modified under all of the experimental conditions employed (Table 2).

3.3. Quantification of oxidation products generated in eGFP in AAPH- or γ-irradiation-treated samples

MetSO, NFKy, Ky, DOPA, and diTyr are products generated after oxidative modifications on Met, Trp and Tyr residues in proteins exposed to one or two-electron oxidants [22,23]. MetSO was quantified by the OPA-precolumn derivatization methodology. Incubation with AAPH 30 and 100 mM led to the formation of 139.3 and 231.5 μM of MetSO, respectively (Table 3). These values mean that 2.1 and 3.5 residues of Met were transformed to MetSO. For γ-irradiated samples, similar values were reported with a total formation of 103.4 and 167.3 μM of MetSO in samples with cumulative doses of 2 kGy and 10 kGy, respectively (Table 3).

To quantify the oxidation products of Trp (NFKy and Ky), and Tyr (DOPA and diTyr), HPLC with fluorescence detection was employed. Since NFKy is hydrolyzed to Ky under acidic conditions [29], these values were reported together (as the sum of both products). As presented in Table 3, 6.2, 10.1 and 2.9 μM of NFKy + Ky, DOPA and diTyr were quantified in samples incubated with AAPH 30 mM. Incubation with AAPH 100 mM led to the formation of 7.9, 11.4 and 5.2 μM of NFKy + Ky, DOPA and diTyr, respectively. These values indicate that 0.1 residues of Trp were modified to NFKy or Ky per eGFP molecule exposed to ROO$^{\bullet}$. In addition, values (expressed per eGFP molecule) ranging between 0.04 and 0.08, and 0.15 and 0.17 were determined for diTyr bonds, and DOPA, respectively. Such results cannot explain the total consumption of Tyr evidenced in AAPH-treated samples. Interestingly, formation of the oxidation products was not linearly related to the changes in the total doses of ROO$^{\bullet}$ achieved with AAPH 30 and 100 mM (288 versus 960 μM [31]). On the other hand, for samples

Table 3
Quantification of the oxidation products of Trp (NFKy + Ky), Tyr (diTyr and DOPA), Met (MetSO), and total protein carbonyls measured after acidic hydrolysis of oxidized samples of eGFP (66 μM). Results are presented in μM, and data correspond to mean values ± standard deviation of at least three independent experiments. Data in parenthesis represent normalized values per molecule of eGFP.

	NFKy + Ky	diTyr	DOPA	MetSO	Protein carbonyls
AAPH 30 mM	6.2 ± 0.9 (0.09)	2.9 ± 0.2 (0.04)	10.1 ± 0.7 (0.15)	139.3 ± 35.6 (2.11)	3.0 ± 0.2 (0.05)
AAPH 100 mM	7.9 ± 0.8 (0.12)	5.2 ± 0.4 (0.08)	11.4 ± 1.1 (0.17)	231.5 ± 37.0 (3.51)	32.2 ± 2.0 (0.49)
2 kGy	2.5 ± 0.3 (0.04)	1.0 ± 0.2 (0.02)	4.1 ± 0.2 (0.06)	103.4 ± 14.6 (1.57)	2.2 ± 0.2 (0.03)
10 kGy	3.2 ± 0.5 (0.05)	0.7 ± 0.2 (0.01)	4.6 ± 0.2 (0.07)	167.3 ± 13.2 (2.54)	16.4 ± 1.2 (0.25)

irradiated with the ^{60}Co-source values of 2.5 and 3.2 μM of NFKy + Ky were found for 2 and 10 kGy samples, respectively (Table 3).

Additionally, Lys consumption was evidenced through OPA-pre-column derivatization methodology (Table 2). This could be explained by formation of Schiff-bases with protein-carbonyls, which also contribute to protein covalent aggregation [25]. To explore this pathway, total carbonyl groups were assessed employing the DNPH-based assay [28]. Samples incubated with AAPH 30 mM, as well as those exposed to the lowest γ-radiation (2 kGy) presented values of 3.0 and 2.2 μM (Table 3). These values were not significantly different from those obtained for control samples. Nonetheless, for samples exposed to higher doses of ROO$^{\bullet}$, and γ-radiation, total protein carbonyls showed a significant increase reaching values of 32.2 and 16.4 μM for AAPH 100 mM and 10 kGy γ-radiation exposure, respectively.

3.4. Detection of diTyr and Tyr-Cys bonds in eGFP oxidized samples by LC-MS

To get more insights regarding the mechanisms involved in the oxidative modifications of eGFP triggered by its exposure to ROO$^{\bullet}$ and free radicals generated from the γ-radiolysis of water, samples were submitted to acidic hydrolysis and then analyzed by LC-MS. This approach have demonstrated to be useful to detect crosslinks such as diTyr and diTrp by LC-MS [25]. However, it is not adequate to determine Schiff-base adducts as these species are susceptible to be hydrolyzed under our experimental conditions [36].

Formation of oxidation products of Tyr, Cys and Trp were searched in full-scan mode (Table 4 summarizes all the detected products). Trp oxidation led to the formation of three products with a +32 Da shift with respect to the parent amino acid (*m/z* 205). These products were identified as Trp-diol/diOia (*m/z* 237) and NFK (*m/z* 237) according to the MS^2 pattern previously reported [30,37,38]. On the other hand, for Tyr and Cys it was not possible to find clear signals of incorporation of one or two oxygen atoms (+16 or +32 Da shift). Nonetheless, MS signals in agreement with the recombination of two Tyr$^{\bullet}$ to generate diTyr bonds (*m/z* 361), and the recombination of a Tyr$^{\bullet}$ with a Cys$^{\bullet}$ to generate Cys-Tyr bonds (*m/z* 301) were evidenced (Table 4). Fig. 3A presents the chromatographic peaks obtained by LC-MS registered at 7.6 and 9.1 min, with a *m/z* value of 361 and a MS^2 pattern in agreement with diTyr. As Fig. 3B shows, fragmentation of the peak registered at 7.6 min resulted in the formation of two principal ions with masses of 344 and 315. These fragments agree with the loss of an amino group (loss of 17 Da) and water plus carbon monoxide groups (loss of 46 Da) [25,39,40]. A similar pattern was registered after the fragmentation of the peak at 9.1 min (Fig. 3C). On the other hand, to confirm the MS and MS^2 pattern of Cys-Tyr bonds, generated as consequence of the eGFP oxidation, a solution containing the mixture of the amino acids Cys (1 mM) and Tyr (1 mM) was incubated with AAPH (100 mM) at 37 °C for 2 h and analyzed by LC-MS. Fig. 4A shows the chromatogram obtained after running the hydrolyzed samples of oxidized eGFP, and the oxidized sample containing free amino acids. For the oxidized amino acids mixture (red line) it was evidenced the formation of two peaks at 1.5 and 7.4 min corresponding to Cys-Cys bonds (*m/z* 241 [41]) and Cys-Tyr bonds (*m/z* 301), respectively. On the other hand, the LC-MS analysis of oxidized eGFP samples, formation of different peaks corresponding to Tyr- and Trp-derived products, was evidenced. Furthermore, amongst the detected peaks only the signal registered at 7.5 min presented a *m/z* of 301. Fig. 4B depicts the MS^2 fragmentation pattern

Table 4
List of products detected by UPLC-MS analysis of oxidized samples of eGFP (66 μM). Protein was either oxidized after incubation with AAPH (100 mM) during 2 h at 37 °C, or after exposure to y-radiation until a dose of 10 kGy was reached. Oxidized samples were hydrolyzed as described in materials and methods section prior to MS-analysis.

Sample	Retention time (min)	*m/z*	MS^2	Assignment
eGFPox (AAPH 100 mM)	6.0	182.1	164.9 (loss of NH_3)	Parent Tyr
	6.1	361.2	344.2 (loss of NH_3)	diTyr
			315.2 (loss of H_2O + CO)	
	6.3	237.1	219.1 (loss of H_2O)	Trp-diol/diOia
			146.0 (loss of $C_2H_3NO_2/H_2O$)	
	7.5	301.1	284.0 (loss of NH_3)	Cys-Tyr
			255.0 (loss of H_2O + CO)	
			212.0 (loss of loss of $C_3H_7NO_2$)	
	7.6	361.2	344.2 (loss of NH_3)	diTyr
			315.2 (loss of H_2O + CO)	
	7.8	237.1	219.1 (loss of H_2O)	Trp-diol/diOia
			146.0 (loss of $C_2H_3NO_2/H_2O$)	
	9.1	361.2	344.2 (loss of NH_3)	diTyr
			315.2 (loss of H_2O + CO)	
	11.1	361.3	344.3 (loss of NH_3)	diTyr
			315.3 (loss of H_2O + CO)	
	11.3	237.2	220.1 (loss of NH_3)	NFKy
			202.2 (loss of NH_3/H_2O)	
			191.1 (loss of H_2O + CO)	
	14.6	205.1	187.9 (loss of NH_3)	Parent Trp
eGFPox (γ-radiation, 10 kGy)	5.9	182.1	165.0 (loss of NH_3)	Parent Tyr
	6.0	361.2	344.2 (loss of NH_3)	diTyr
			315.2 (loss of H_2O + CO)	
	6.5	237.1	219.1 (loss of H_2O)	Trp-diol/diOia
			146.1 (loss of $C_2H_3NO_2/H_2O$)	
	7.4	301.2	284.0 (loss of NH_3)	Cys-Tyr
			255.0 (loss of H_2O + CO)	
			212.0 (loss of $C_3H_7NO_2$)	
	8.8	361.3	344.3 (loss of NH_3)	diTyr
			315.3 (loss of H_2O + CO)	
	10.8	361.4	344.4 (loss of NH_3)	diTyr
			315.4 (loss of H_2O + CO)	
	11.4	237.2	220.2 (loss of NH_3)	NFKy
			202.2 (loss of NH_3/H_2O)	
	14.6	205.1	188.1 (loss of NH_3)	Parent Trp

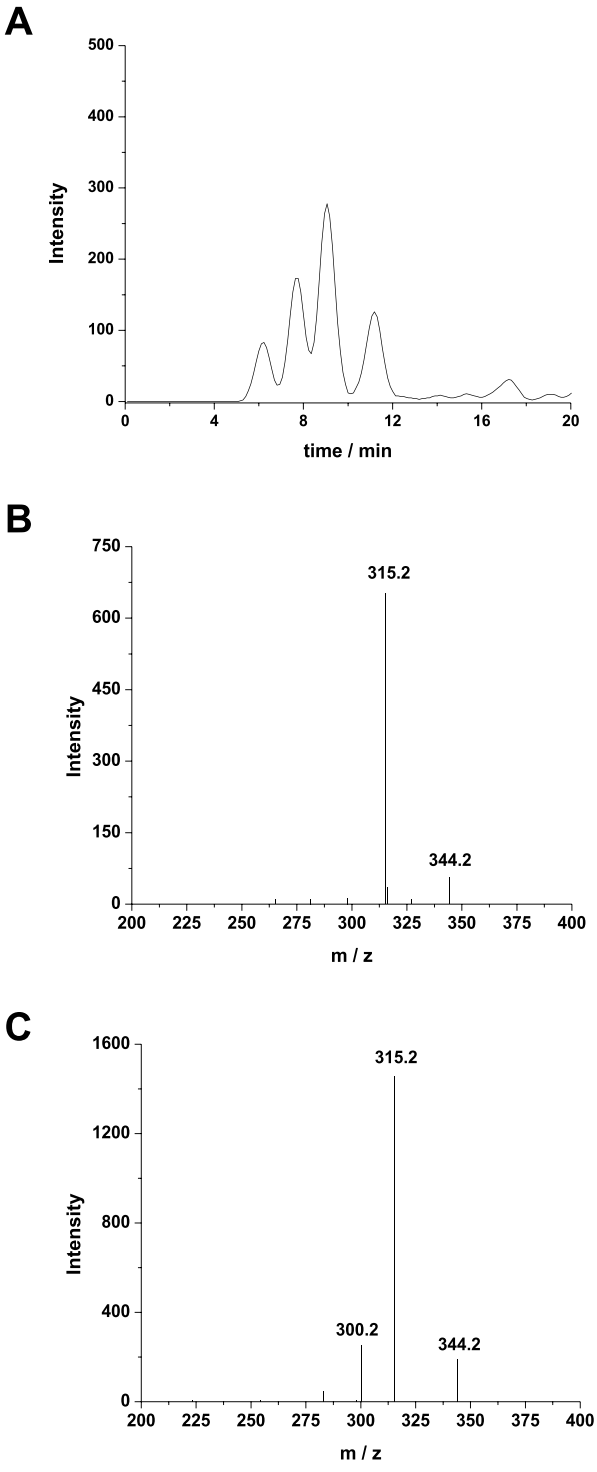

Fig. 3. Detection of diTyr bonds generated as consequence of eGFP (66 μM) incubation with AAPH 100 mM during 2 h at 37 °C in phosphate buffer saline (75 mM, pH 7.4). Oxidized eGFP samples were submitted to acid hydrolysis as described in materials and methods section before injection into a LC-MS/MS system. Panel A: chromatogram obtained for *m/z* 361 (mass of diTyr bonds). Panel B: MS/MS of the peak registered at 7.6 min. Panel C: MS/MS of the peak registered at 9.1 min.

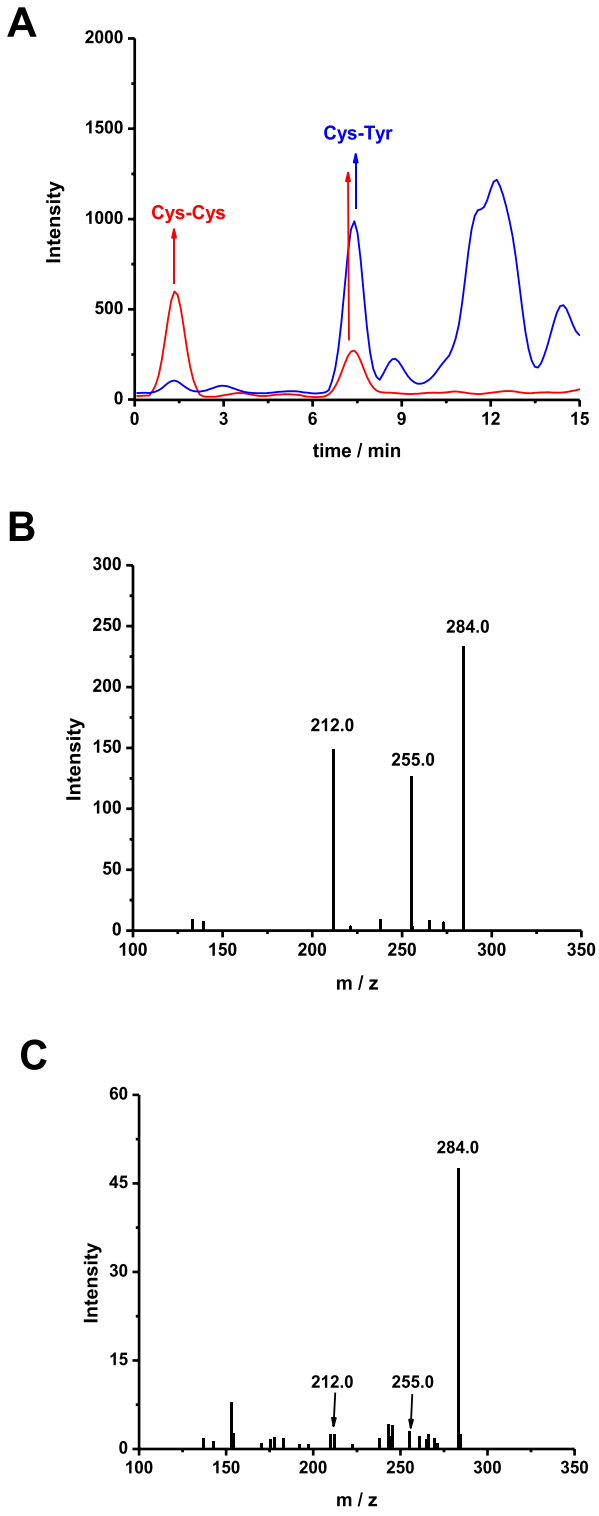

Fig. 4. Incubation of eGFP with APPH at 37 °C results in formation of Cys-Tyr bonds. Oxidized proteins samples (66 μM incubated with AAPH 100 mM during 120 min) were submitted to acid hydrolysis and then analyzed by LC-MS/MS. To have a proper confirmation of Cys-Tyr bonds formation, a solution containing Tyr (1 mM) and Cys (1 mM) was incubated with AAPH (100 mM) at 37 °C and was also analyzed by LC-MS/MS. Panel A: chromatogram obtained at *m/z* 301 in eGFP oxidized samples (blue line) and for Cys + Tyr oxidized sample (red line). Panel B: MS/MS of the peak registered at 7.4 min (*m/z* 301) in Cys + Tyr oxidized samples. Panel C: MS/MS of the peak registered at 7.5 min (*m/z* 301) in eGFP oxidized samples. (For interpretation of the references to colour in this figure legend, the reader is referred to the Web version of this article.)

of the peak registered at 7.4 min corresponding to the Cys-Tyr bonds. Formation of the fragments with masses of 284 (loss of 17 Da) and 255 (loss of 46 Da) are in agreement with loss of an amino group and water plus carbon monoxide groups, respectively. Both fragmentation patterns correspond to the major losses of protonated Cys- and Tyr-derived

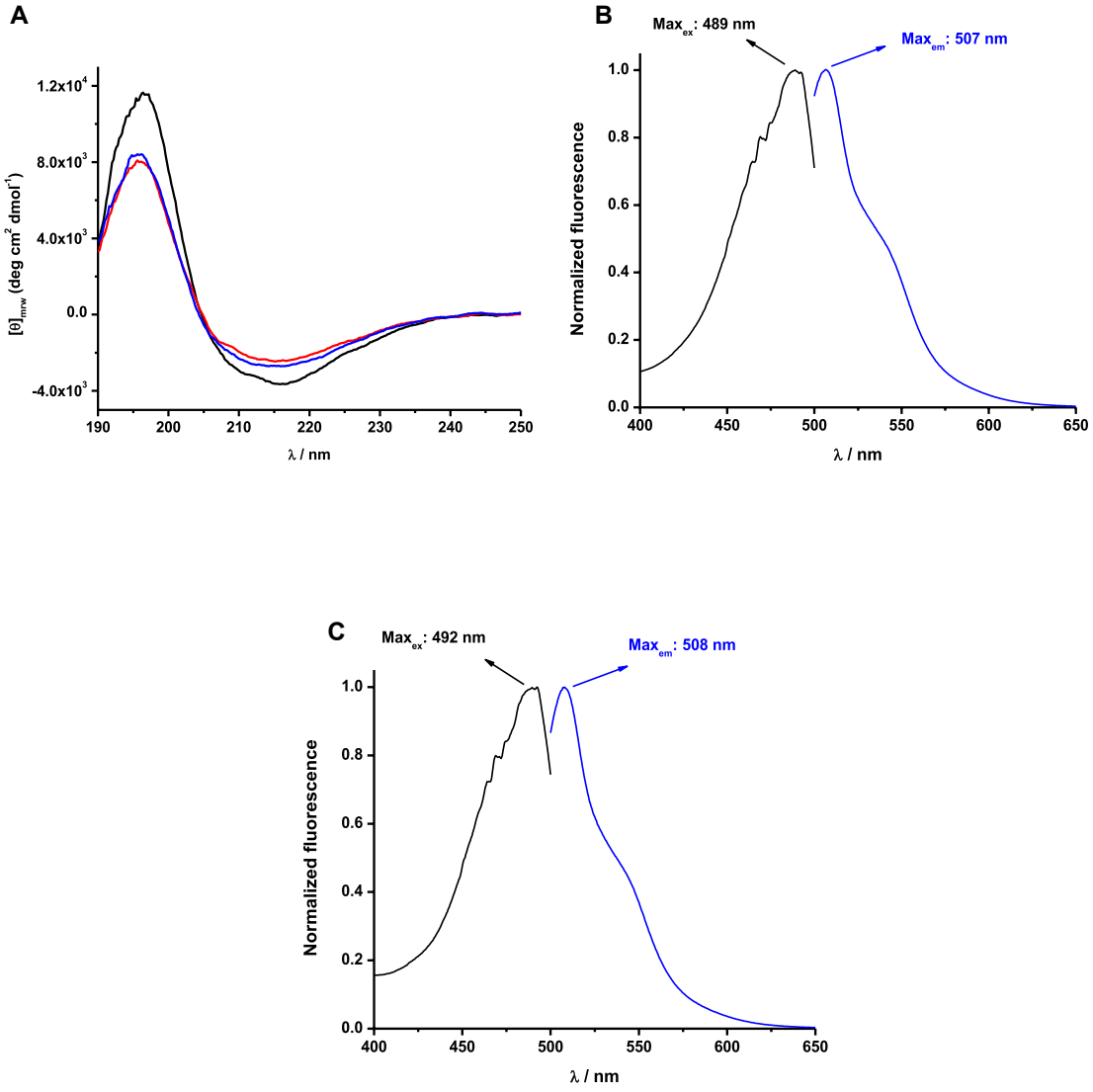

Figure 5

Fig. 5. Peroxyl radical mediated oxidation of eGFP does not alter significantly the conformational and spectral properties of the protein with regards to its native monomeric form. Panel A: far-UV CD spectrum of control eGFP (66 μM) sample is presented with a black line, whereas oxidized samples obtained after incubation (2h) of eGFP (66 μM) with AAPH 30 or 100 mM at 37 °C are presented with red and blue lines, respectively. Panel B: Excitation (black line) and emission (blue line) spectrum of oxidized monomeric eGFP. Panel C: Excitation (black line) and emission (blue line) spectrum of oxidized dimeric eGFP. Both oxidized monomeric and dimeric eGFP were obtained as described in materials and methods section after separation by size exclusion chromatography of samples incubated with AAPH 100 mM during 2 h at 37 °C. (For interpretation of the references to colour in this figure legend, the reader is referred to the Web version of this article.)

molecules [39,40]. In addition, a third fragment with a mass of 212 (loss of 89 Da) was generated. This loss is in agreement with formation of Cys-derived products where C–S cleavage can be evidenced [42,43]. This fragmentation was also evidenced after MS^2 analysis of the peak with m/z 301 registered at 7.5 min in hydrolyzed eGFP oxidized samples confirming the formation of Cys-Tyr bonds (Fig. 4C).

3.5. Detection of fluorescent soluble cross-links of eGFP

To get a better understanding of the structural and fluorescent consequences of exposure of eGFP to free radicals generated from γ-radiolysis of water and thermolysis of AAPH, oxidized samples were centrifuged at 14,000 rpm in order to separate the soluble fraction. These samples were then injected into a HPLC system employing a size-exclusion column. Only the monomeric and dimeric forms of eGFP evidenced solubility in aqueous medium (Supplementary Fig. 3).

Far-UV CD experiments of the soluble fraction of ROO•-treated samples showed little changes in the spectra (Fig. 5A). On the contrary, upon exposure to γ-radiation, a significant modification on the Far UV-CD spectra was observed for samples exposed to the highest dose of γ-irradiation (10 kGy), implying changes at level of secondary structure of eGFP (Supplementary Fig. 7).

Finally, the fluorescence spectrum of the native eGFP, and the oxidized monomeric and dimeric species produced after ROO•-mediated oxidation of the protein were studied. As Fig. 5B depicts, oxidized monomeric eGFP, showed an excitation and emission spectrum with maximums at 489 and 507 nm, respectively. This fluorescent behavior was similar to the evidenced for non-oxidized monomeric eGFP (Supplementary Fig. 2). Moreover, the fluorescent properties of the dimeric oxidized eGFP showed a small red shift of 2 nm for the excitation spectrum and 1 nm for the emission spectrum of the protein (Fig. 5C). Similar findings with small shifts in the excitation and emission spectrum of eGFP have been reported for non-covalent oligomers of eGFP [11].

4. Discussion

The presence of oxidizable residues in the eGFP structure; Tyr, Met, Trp and Cys, makes this protein prone to accumulate oxidative damage. Such damage firstly involves the formation of Tyr• and Trp•, which are believed to play a key role in protein oxidation since these species can react with O_2 (or $O_2^{\bullet-}$) to give several oxygenated products (e.g. hydroperoxides, alcohols and carbonyls) [22,23,44–46]. Additionally, Tyr•, Trp• and Cys• can participate in self-reactions to give intra- or inter-molecular diTyr, diTrp, and cystine bonds, mediating protein cross-linking [22,24,45,47]. Furthermore, once Tyr• and Trp• are generated, the cross-reaction between them can occur to give Tyr-Trp bonds as evidenced for Glucose-6-phosphate dehydrogenase and lysozyme [29,48,49]. Based on the well-known structure of eGFP [5,11], we hypothesized that its exposure to AAPH-derived ROO• and free radicals generated from γ-radiolysis of water would induce the oxidation of susceptible residues leading to the generation of secondary free radicals that can mediate eGFP cross-linking affecting its fluorescence spectrum.

Exposure of eGFP to AAPH-derived ROO•, and to the mixture of free radicals that are generated during γ-radiolysis of water, resulted in a considerable consumption of its monomer (Table 1). This consumption was accompanied by the formation of different crosslinked species for AAPH-treated samples, whilst γ-irradiation exposure led to the formation of eGFP smeared bands with evidence of dimeric species (Fig. 1). The difference in the SDS-PAGE pattern of the oxidative modifications elicited by these oxidative sources can be explained by the chemical properties of the oxidants involved and the total amount of radicals introduced in the system. Thus, while thermolysis of AAPH generates ROO•, a mild oxidant (E° = 1.0 V [21]) that reacts selectively with the side chain of specific residues (i.e. Cys, Trp, Tyr, Met and His [22,50]), γ-radiolysis of water generates a mixture of oxidants including •OH, H_2O_2 and $O_2^{\bullet-}$ [33]. Of these oxidants, •OH is highly oxidizing (E° = 2.3 V [21]) and reacts rapidly and unespecifically with the side chain of most amino acids [23]. This lack of specificity of •OH leads to the formation of several products in the side chain of the amino acids of which not all participate in crosslinking pathways. Moreover, it is well-known that protein crosslinking depends on the generation, and recombination, of a pair of secondary free radicals. Thus, in spite that these reactions occurs very rapidly with kinetic constants in the order of 10^9 $M^{-1}s^{-1}$ for Tyr•-Tyr• and Trp•-Trp• recombination [24,47], under aerobic environment the predominant products correspond to hydroperoxides and other oxygenated products [22]. This scenario is increased by the formation of $O_2^{\bullet-}$ in the medium for γ-irradiation treated samples. In fact, $O_2^{\bullet-}$ rise the ratio of formation of hydroperoxides and other oxygenated products of Trp and Tyr since its reaction with Trp• and Tyr• also present kinetic rates in the order of 10^9 $M^{-1}s^{-1}$ [46,47]. Taking this into consideration, it is clear that in spite that the total amount of •OH (2.798 μmol) generated after γ-irradiation (10 kGy) was ~ 3-fold greater than the amount of ROO• generated with AAPH 100 mM (0.96 μmol), formation of other oxidants during γ-radiolysis of water would interfere with formation of crosslinks explaining the different between the two oxidative systems. Therefore, in spite that oxidation mediated by free radicals from γ-radiolysis of water triggered a major consumption of the eGFP monomer (Table 1), ROO•-mediated oxidation was more efficient inducing the formation of eGFP dimers, trimers and protein crosslinks with higher molecular masses (Fig. 1). In fact, after exposure to ROO• (15 min) the fast formation of dimers and trimers of eGFP would indicate that recombination of secondary free radicals leading to protein cross-linking may be occurring. A similar behavior, where fast cross-linking of β-casein was evidenced after exposure to oxidative sources, was associated to the recombination of secondary free radicals as principal pathway [25,51]. Nonetheless, it cannot be discarded that at longer incubation times other pathways different to the recombination of secondary free radicals may be also involved in the cross-linking of eGFP as evidenced for α- and β-casein [25].

In addition to the formation of the dimers and other higher molecular mass crosslinks of eGFP evidenced by SDS-PAGE in samples treated with AAPH 30 mM (Fig. 1), it was evidenced the formation of bands with masses between 30 and 50 kDa. These species correspond to eGFP crosslinks with greater masses than the monomer but lesser than the dimers. From these results we speculate that protein crosslinking between the monomer with fragments of eGFP is occurring. This is supported by the presence of peaks with higher retention times than the monomer in HPLC-DAD experiments employing a SEC column (Fig. 2) implying formation of species with lower molecular masses than the monomer. Similar findings were reported by Arenas et al. (2013) after Lysozyme oxidation mediated by AAPH-derived ROO• [52]. Furthermore, since SDS-PAGE showed a fast generation of eGFP dimers and trimers, the formation of reducible bonds (i.e. disulfide bonds) was studied by SDS-PAGE under reducing and non-reducing conditions (Fig. 1 and Supplementary Fig. 4, respectively). In spite of that eGFP has two free thiols in its primary structure, of which Cys48 is located on the surface of the protein [53], no big differences between reducing and non-reducing electrophoretic gels was observed with the exemption of the species between 30 and 50 kDa for samples treated with AAPH 30 mM. This clearly indicates that formation of disulfide bonds is not a principal pathway of eGFP cross-linking mediated by ROO• and free radicals from γ-radiolysis. This result was supported by LC-MS analysis of hydrolyzed samples, where cystine was not found neither in AAPH- or γ-irradiation-treated samples.

To have a further understanding on the pathways leading to the modifications in the molecular mass of eGFP, studies aimed to determine the extent of Tyr and Trp consumption, and formation their oxidation products were performed. Results showed that regardless of that incubation with AAPH 100 mM leaded to a significant consumption of Tyr (Table 2), only modest levels of its oxidation products (DOPA and diTyr) were detected (Table 3). Moreover, in addition to Tyr consumption, loss of Met was evidenced. Met consumption was in concordance with the levels of MetSO detected which correspond to the majoritarian product of Met oxidation under aerobic environments [54]. The later was reflected, for example, in the formation of 3.5 and 2.5 molecules of MetSO per eGFP molecule in samples incubated with AAPH 100 mM and exposed to 10 kGy, respectively. These values mean that 90% and 96% of the total Met consumed in these conditions led to formation of MetSO, respectively (Tables 2 and 3). Interestingly, along with the significant oxidation of Tyr and Met, loss of Lys was also determined (Table 2). This residue is not a target of ROO•, but the nucleophilic amine group of its side chain can react with secondary products (e.g. carbonyl groups) generated in the side chain of Trp, Tyr or His [22,55]. In fact, detection and quantification of carbonyl groups after ROO•-mediated oxidation of eGFP (Table 3) support the occurrence of this kind of reactions. Thus, the nucleophilic attack from the

amine group of Lys to the carbonyl group will trigger the formation of Schiff bases which can also participate in the cross-linking of eGFP. This kind of reactions has been reported in the cross-linking and covalent aggregation of other proteins such as β-casein and eye lens proteins [25,56,57]. On the contrary, regardless the fact that γ-irradiation-induced oxidation was also accompanied by a loss of Lys residues and carbonyl groups formation (Tables 2 and 3), we cannot link this evidence to eGFP crosslinking through Schiff base formation since $^{\bullet}OH$ is capable of directly oxidize this residue [23]. The latter is a consequence of the high reactivity of $^{\bullet}OH$ which makes this oxidant capable of oxidizing Lys, and thus its consumption might be associated to a direct oxidation and not secondary processes [22].

As formation of DOPA and diTyr only represented a fraction of the total consumption of Tyr, and NFKy and Ky would only represent a fraction of the total products that can be generated during Trp oxidation, LC-MS analyses were carried out to investigate the formation of other oxidation products derived from these amino acids. These results showed the formation of two new products of Trp but none of them corresponded to diTrp bonds (Table 4). In spite that recent works have demonstrated formation of diTrp bonds in cross-linked proteins [24,49,58], this dimer was not observed under our experimental conditions. Probably the sterically hindered location of the single Trp residue inside the beta-barrel of eGFP limits self-reactions of $Trp^{\bullet}$ [34]. The detection of only 3 Trp products by LC-MS, along with the quantification of values between 0.04 and 0.12 NFKy + Ky produced per eGFP molecule, indicates that the single Trp residue of eGFP would be only partially modified in $ROO^{\bullet}$ and $^{\bullet}OH$ oxidized samples (Tables 3 and 4). For Tyr instead, in agreement with quantification by UPLC-methodologies, LC-MS analyses confirmed the formation of diTyr bonds after exposure of eGFP to $ROO^{\bullet}$ (Fig. 3). Interestingly, along with the detection of diTyr bonds, a clear signal with $m/z = 301$ was detected in these samples (Fig. 4). This signal was assigned to Cys-Tyr bonds generated during the eGFP oxidation (Fig. 4 and Table 4). Formation of such species has been evidenced in the catalytic site of different metalloproteins as consequence of post-translational modifications. In these proteins, formation of Cys-Tyr crosslinks can occur under aerobic or anaerobic conditions as demonstrated for Galactose oxidase, Cysteine dioxygenase and the orphan metalloprotein BF4112 [59–63]. In metalloproteins, Cys-Tyr crosslinking firstly involves the formation of $Cys^{\bullet}$ or $Tyr^{\bullet}$ triggered by redox active metals. Recombination of such secondary free radicals leads to Cys-Tyr bonds [63]. Notwithstanding that eGFP does not contain transition metals in its structure, $Cys^{\bullet}$ and $Tyr^{\bullet}$ can be formed by exposure towards $ROO^{\bullet}$. Thus, along with diTyr bonds, Cys-Tyr crosslinks could also be mediating the intra- or intermolecular crosslinking of eGFP. Intermolecular Cys-Tyr bonds could be favored since Cys48 and four Tyr residues are located in the surface of the protein meaning that recombination of a secondary free radical of Cys48 formed in an eGFP molecule could react with a $Tyr^{\bullet}$ formed in a second eGFP molecule (Supplementary Fig. 8).

Interestingly, in spite that γ-irradiation-mediated eGFP oxidation led to a minor extent of Tyr consumption and protein cross-linking than the processes induced by $ROO^{\bullet}$, diTyr and Cys-Tyr crosslinks were also detected by LC-MS (Table 4). Nonetheless, as evidenced by circular dichroism, and in agreement with the smeared band observed in SDS-PAGE, oxidants generated from γ-radiolysis of water would induce significant changes in the secondary structure of the protein when samples were irradiated until a dose of 10 kGy was achieved (Supplementary Fig. 7). This could be attributed to the oxidation mediated by $^{\bullet}OH$ due its high reactivity. Contrarily to $ROO^{\bullet}$, the changes induced by free radicals generated after γ-radiolysis triggered a total loss of the fluorescence signal arising from the eGFP chromophore (data not shown). Notwithstanding the aforementioned, this was not the case for AAPH-treated samples. After incubation with AAPH (30 and 100 mM) during 3 h at 37 °C, no big changes on the secondary structure of the protein were evinced (Fig. 5). Moreover, the fluorescence spectrum of the oxidized monomeric and dimeric eGFP species did not changed with respect to the non-oxidized monomeric eGFP (Supplementary Fig. 2). These results confirm that exposure of eGFP to oxidants generated in cellular milieus will trigger formation of intermolecular crosslinks. Crosslinking would occur through a mixture of radical-radical self-reactions with diTyr and Cys-Tyr bonds formation, and secondary reactions involving Lys residues and carbonyl groups generated in the side chain of Trp or Tyr residues. These crosslinks, as well as the oxidized monomer, maintains the secondary structure and the fluorescent spectrum of the chromophore of eGFP. The latter might lead to the formation of potential artifacts inside the cell. For example, in studies aimed to investigate the cross-talk and/or localization of tagged molecules, homo-dimeric species eGFP might lead to think that the two tagged molecules are interacting when the co-localization is due to the oxidative crosslinking of the fluorescent protein instead. The latter arises from the fact that both eGFP-monomer and eGFP-homodimer present a similar fluorescence spectrum which is hard to differentiate. Overall, our results demonstrate the importance of controlling the experimental set up when using fluorescent proteins as tags.

5. Conclusion

The eGFP is susceptible to accumulate oxidative damage induced by reactive species that are generated in biological milieus. This damage trigger the consumption of the eGFP monomer with protein crosslinking being the principal pathway of modification. Depending on the oxidative source, this oxidative damage can cause the complete loss of its fluorescence or lead to the formation of soluble dimers that conserve the fluorescence spectrum of the native eGFP chromophore.

Acknowledgements

This work was supported by FONDECYT N° 1190881, 1191321, and by FONDEQUIP N° EQM 120065. RZ thanks to DICYT 021741AL_POSTDOC, EFL thanks to DICYT 021941AL_POSTDOC, PB thanks to CONICYT for PhD Doctorate fellowship (21160605), and FM thanks to FONDECYT postdoctorate fellowship (3170590). CD spectroscopy was performed in equipment supported by FONDEQUIP N° EQM 140151.

Appendix A. Supplementary data

Supplementary data to this article can be found online at https://doi.org/10.1016/j.freeradbiomed.2020.02.006.

References

[1] M. Chalfie, S. Kain, Green Fluorescent Protein : Properties, Applications, and Protocols, Wiley, 0471736821, 2006.
[2] D.M. Chudakov, M.V. Matz, S. Lukyanov, K.A. Lukyanov, Fluorescent proteins and their applications in imaging living cells and tissues, Physiol. Rev. 90 (2010) 1103–1163, https://doi.org/10.1152/physrev.00038.2009.
[3] L. Kallal, J.L. Benovic, Using green fluorescent proteins to study G-protein-coupled receptor localization and trafficking, Trends Pharmacol. Sci. 21 (2000) 175–180, https://doi.org/10.1016/S0165-6147(00)01477-2.
[4] A.S. Mishin, V.V. Belousov, K.M. Solntsev, K.A. Lukyanov, Novel uses of fluorescent proteins, Curr. Opin. Chem. Biol. 27 (2015) 1–9, https://doi.org/10.1016/J.CBPA.2015.05.002.
[5] U. Haupts, S. Maiti, P. Schwille, W.W. Webb, Dynamics of fluorescence fluctuations in green fluorescent protein observed by fluorescence correlation spectroscopy, Proc. Natl. Acad. Sci. U. S. A. 95 (1998) 13573–13578, https://doi.org/10.1073/PNAS.95.23.13573.
[6] H. Shinoda, M. Shannon, T. Nagai, Fluorescent proteins for investigating biological events in acidic environments, Int. J. Mol. Sci. 19 (2018) 1548, https://doi.org/10.3390/ijms19061548.
[7] J.A.J. Arpino, P.J. Rizkallah, D.D. Jones, Crystal structure of enhanced green fluorescent protein to 1.35 Å resolution reveals alternative conformations for Glu222, PloS One 7 (2012) 47132, https://doi.org/10.1371/journal.pone.0047132.
[8] R.M. Wachter, The family of GFP-like proteins: structure, function, photophysics and biosensor applications. Introduction and perspective, Photochem. Photobiol. 82 (2006) 339–344, https://doi.org/10.1562/2005-10-02-IR-708.
[9] S.J. Remington, Green fluorescent protein: a perspective, Protein Sci. 20 (2011)

1509–1519, https://doi.org/10.1002/pro.684.
[10] E.A. Specht, E. Braselmann, A.E. Palmer, A Critical and comparative review of fluorescent tools for live-cell imaging, Annu. Rev. Physiol. 79 (2017) 93–117, https://doi.org/10.1146/annurev-physiol-022516-034055.
[11] G. Vámosi, N. Mücke, G. Müller, J.W. Krieger, U. Curth, J. Langowski, K. Tóth, EGFP oligomers as natural fluorescence and hydrodynamic standards, Sci. Rep. 6 (2016) 33022, https://doi.org/10.1038/srep33022.
[12] E.L. Snapp, R.S. Hegde, M. Francolini, F. Lombardo, S. Colombo, E. Pedrazzini, N. Borgese, J. Lippincott-Schwartz, Formation of stacked ER cisternae by low affinity protein interactions, J. Cell Biol. 163 (2003) 257–269, https://doi.org/10.1083/jcb.200306020.
[13] D.A. Zacharias, J.D. Violin, A.C. Newton, R.Y. Tsien, Partitioning of lipid-modified monomeric GFPs into membrane microdomains of live cells, Science 296 (2002) 913–916, https://doi.org/10.1126/science.1068539.
[14] E. Snapp, Design and use of fluorescent fusion proteins in cell biology, Curr. Protoc. Cell Biol. 27 (2005) 21.4.1–21.4.13, https://doi.org/10.1002/0471143030.cb2104s27.
[15] D. Ganini, F. Leinisch, A. Kumar, J. Jiang, E.J. Tokar, C.C. Malone, R.M. Petrovich, R.P. Mason, Fluorescent proteins such as eGFP lead to catalytic oxidative stress in cells, Redox Biol. 12 (2017) 462–468, https://doi.org/10.1016/J.REDOX.2017.03.002.
[16] R. Heim, D.C. Prasher, R.Y. Tsien, Wavelength mutations and posttranslational autoxidation of green fluorescent protein, Proc. Natl. Acad. Sci. U. S. A. 91 (1994) 12501–12504, https://doi.org/10.1073/pnas.91.26.12501.
[17] A.J. Trewin, B.J. Berry, A.Y. Wei, L.L. Bahr, T.H. Foster, A.P. Wojtovich, Light-induced oxidant production by fluorescent proteins, Free Radic. Biol. Med. 128 (2018) 157–164, https://doi.org/10.1016/J.FREERADBIOMED.2018.02.002.
[18] B. Halliwell, J.M.C. Gutteridge, Free Radicals in Biology and Medicine, Oxford University Press, 2015, https://doi.org/10.1093/acprof:oso/9780198717478.001.0001.
[19] B.C. Dickinson, C.J. Chang, Chemistry and biology of reactive oxygen species in signaling or stress responses, Nat. Chem. Biol. 7 (2011) 504–511, https://doi.org/10.1038/nchembio.607.
[20] F.A. Villamena, Chemistry of reactive species, Mol. Basis Oxidative Stress, John Wiley & Sons, Inc., Hoboken, NJ, USA, 2013, pp. 1–48, , https://doi.org/10.1002/9781118355886.ch1.
[21] G.R. Buettner, The pecking order of free radicals and antioxidants: lipid peroxidation, α-Tocopherol, and ascorbate, Arch. Biochem. Biophys. 300 (1993) 535–543, https://doi.org/10.1006/ABBI.1993.1074.
[22] M.J. Davies, Protein oxidation and peroxidation, Biochem. J. 473 (2016) 805–825, https://doi.org/10.1042/BJ20151227.
[23] M.J. Davies, The oxidative environment and protein damage, Biochim. Biophys. Acta Protein Proteonomics 1703 (2005) 93–109, https://doi.org/10.1016/J.BBAPAP.2004.08.007.
[24] L. Carroll, D.I. Pattison, J.B. Davies, R.F. Anderson, C. Lopez-Alarcon, M.J. Davies, Formation and detection of oxidant-generated tryptophan dimers in peptides and proteins, Free Radic. Biol. Med. 113 (2017) 132–142, https://doi.org/10.1016/J.FREERADBIOMED.2017.09.020.
[25] E. Fuentes-Lemus, E. Silva, P. Barrias, A. Aspee, E. Escobar, L.G. Lorentzen, L. Carroll, F. Leinisch, M.J. Davies, C. López-Alarcón, Aggregation of α- and β-caseins induced by peroxyl radicals involves secondary reactions of carbonyl compounds as well as di-tyrosine and di-tryptophan formation, Free Radic. Biol. Med. 124 (2018) 176–188, https://doi.org/10.1016/J.FREERADBIOMED.2018.06.005.
[26] L. Lindborg, H. Svensson, K.A. Johansson, Procedures in external radiation therapy dosimetry with electron and photon beams with maximum energies between 1 and 50 MeV, Acta Radiol. Oncol. Radiat. Ther. Phys. Biol. 19 (1980) 55–79, https://doi.org/10.3109/02841868009130136.
[27] L.O. Mattsson, K.A. Johansson, H. Svensson, Ferrous sulphate dosimeter for control of ionization chamber dosimetry of electron and60co gamma beams, Acta Oncol. (Madr) 21 (1982) 139–144, https://doi.org/10.3109/02841868209133997.
[28] C.L. Hawkins, P.E. Morgan, M.J. Davies, Quantification of protein modification by oxidants, Free Radic. Biol. Med. 46 (2009) 965–988, https://doi.org/10.1016/J.FREERADBIOMED.2009.01.007.
[29] F. Leinisch, M. Mariotti, M. Rykaer, C. Lopez-Alarcon, P. Hägglund, M.J. Davies, Peroxyl radical- and photo-oxidation of glucose 6-phosphate dehydrogenase generates cross-links and functional changes via oxidation of tyrosine and tryptophan residues, Free Radic. Biol. Med. 112 (2017) 240–252, https://doi.org/10.1016/J.FREERADBIOMED.2017.07.025.
[30] E. Silva, P. Barrias, E. Fuentes-Lemus, C. Tirapegui, A. Aspee, L. Carroll, M.J. Davies, C. López-Alarcón, Riboflavin-induced Type 1 photo-oxidation of tryptophan using a high intensity 365 nm light emitting diode, Free Radic. Biol. Med. 131 (2019) 133–143, https://doi.org/10.1016/J.FREERADBIOMED.2018.11.026.
[31] E. Niki, [3] Free radical initiators as source of water- or lipid-soluble peroxyl radicals, Methods Enzymol. 186 (1990) 100–108, https://doi.org/10.1016/0076-6879(90)86095-D.
[32] J.A. LaVerne, OH Radicals and oxidizing products in the gamma radiolysis of water, Radiat. Res. 153 (2000) 196–200, https://doi.org/10.1667/0033-7587(2000)153[0196:oraopi]2.0.co;2.
[33] S.I. Borrely, A.C. Cruz, N.L. Del Mastro, M.H.O. Sampa, E.S. Somessari, Radiation processing of sewage and sludge. A review, Prog. Nucl. Energy 33 (1998) 3–21, https://doi.org/10.1016/s0149-1970(97)87287-3.
[34] O. V Stepanenko, O. V Stepanenko, I.M. Kuznetsova, V. V Verkhusha, K.K. Turoverov, Beta-barrel scaffold of fluorescent proteins: folding, stability and role in chromophore formation, Int. Rev. Cell Mol. Biol. 302 (2013) 221–278, https://doi.org/10.1016/B978-0-12-407699-0.00004-2.
[35] M.P. Bartolomeo, F. Maisano, Validation of a reversed-phase HPLC method for quantitative amino acid analysis, J. Biomol. Tech. 17 (2006) 131–137.
[36] E.H. Cordes, W.P. Jencks, On the mechanism of schiff base formation and hydrolysis, J. Am. Chem. Soc. 84 (1962) 832–837, https://doi.org/10.1021/ja00864a031.
[37] M. Gracanin, C.L. Hawkins, D.I. Pattison, M.J. Davies, Singlet-oxygen-mediated amino acid and protein oxidation: formation of tryptophan peroxides and decomposition products, Free Radic. Biol. Med. 47 (2009) 92–102, https://doi.org/10.1016/J.FREERADBIOMED.2009.04.015.
[38] G.E. Ronsein, M.C.B. de Oliveira, M.H.G. de Medeiros, P. Di Mascio, Mechanism of dioxindolylalanine formation by singlet molecular oxygen-mediated oxidation of tryptophan residues, Photochem. Photobiol. Sci. 10 (2011) 1727–1730, https://doi.org/10.1039/c1pp05181d.
[39] H. El Aribi, G. Orlova, A.C. Hopkinson, K.W.M. Siu, Gas-phase Fragmentation Reactions of Protonated Aromatic Amino Acids: Concomitant and Consecutive Neutral Eliminations and Radical Cation Formations, (2004), pp. 3844–3853, https://doi.org/10.1021/JP0374915.
[40] S.-S. Choi, M.J. Song, O.-B. Kim, Y. Kim, Fragmentation patterns of protonated amino acids formed by atmospheric pressure chemical ionization, Rapid Commun. Mass Spectrom. 27 (2013) 143–151, https://doi.org/10.1002/rcm.6411.
[41] P. Zhang, W. Chan, I.L. Ang, R. Wei, M.M.T. Lam, K.M.K. Lei, T.C.W. Poon, Gas-Phase Fragmentation reactions of protonated cystine using high-resolution tandem mass spectrometry, Molecules 24 (2019) 747, https://doi.org/10.3390/molecules24040747.
[42] H. Lioe, R.A.J. O'Hair, Comparison of collision-induced dissociation and electron-induced dissociation of singly protonated aromatic amino acids, cystine and related simple peptides using a hybrid linear ion trap–FT-ICR mass spectrometer, Anal. Bioanal. Chem. 389 (2007) 1429–1437, https://doi.org/10.1007/s00216-007-1535-1.
[43] C.H. Oberth, A.D. Jones, Fragmentation of protonated thioether conjugates of acrolein using low collision energies, J. Am. Soc. Mass Spectrom. 8 (1997) 727–736, https://doi.org/10.1016/S1044-0305(97)00032-9.
[44] L.P. Candeias, P. Wardman, R.P. Mason, The reaction of oxygen with radicals from oxidation of tryptophan and indole-3-acetic acid, Biophys. Chem. 67 (1997) 229–237, https://doi.org/10.1016/s0301-4622(97)00052-5.
[45] E.P.L. Hunter, M.F. Desrosiers, M.G. Simic, The effect of oxygen, antioxidants, and superoxide radical on tyrosine phenoxyl radical dimerization, Free Radic. Biol. Med. 6 (1989) 581–585, https://doi.org/10.1016/0891-5849(89)90064-6.
[46] L. Carroll, D.I. Pattison, J.B. Davies, R.F. Anderson, C. Lopez-Alarcon, M.J. Davies, Superoxide radicals react with peptide-derived tryptophan radicals with very high rate constants to give hydroperoxides as major products, Free Radic. Biol. Med. 118 (2018) 126–136, https://doi.org/10.1016/j.freeradbiomed.2018.02.033.
[47] C. Houée-Lévin, K. Bobrowski, L. Horakova, B. Karademir, C. Schöneich, M.J. Davies, C.M. Spickett, Exploring oxidative modifications of tyrosine: an update on mechanisms of formation, advances in analysis and biological consequences, Free Radic. Res. 49 (2015) 347–373, https://doi.org/10.3109/10715762.2015.1007968.
[48] E. Fuentes-Lemus, M. Mariotti, P. Hägglund, F. Leinisch, A. Fierro, E. Silva, C. López-Alarcón, M.J. Davies, Binding of rose bengal to lysozyme modulates photooxidation and cross-linking reactions involving tyrosine and tryptophan, Free Radic. Biol. Med. 143 (2019) 375–386, https://doi.org/10.1016/J.FREERADBIOMED.2019.08.023.
[49] E.D. Savina, Y.P. Tsentalovich, P.S. Sherin, UV-A induced damage to lysozyme via Type I photochemical reactions sensitized by kynurenic acid, Free Radic. Biol. Med. (2019), https://doi.org/10.1016/j.freeradbiomed.2019.11.017.
[50] C. López-Alarcón, C. Rocco, E. Lissi, C. Carrasco, J.A. Squella, L. Nuñez-Vergara, H. Speisky, Reaction of 5-aminosalicylic acid with peroxyl radicals: Protection and recovery by ascorbic acid and amino acids, Pharm. Res. (N. Y.) 22 (2005) 1642–1648, https://doi.org/10.1007/s11095-005-6948-y.
[51] E. Fuentes-Lemus, E. Silva, F. Leinisch, E. Dorta, L.G. Lorentzen, M.J. Davies, C. López-Alarcón, α- and β-casein aggregation induced by riboflavin-sensitized photo-oxidation occurs via di-tyrosine cross-links and is oxygen concentration dependent, Food Chem. 256 (2018) 119–128, https://doi.org/10.1016/j.foodchem.2018.02.090.
[52] A. Arenas, C. López-Alarcón, M. Kogan, E. Lissi, M.J. Davies, E. Silva, Chemical modification of lysozyme, glucose 6-phosphate dehydrogenase, and bovine eye lens proteins induced by peroxyl radicals: role of oxidizable amino acid residues, Chem. Res. Toxicol. 26 (2013) 67–77, https://doi.org/10.1021/tx300372t.
[53] A. Royant, M. Noirclerc-Savoye, Stabilizing role of glutamic acid 222 in the structure of Enhanced Green Fluorescent protein, J. Struct. Biol. 174 (2011) 385–390, https://doi.org/10.1016/J.JSB.2011.02.004.
[54] C. Schöneich, Methionine oxidation by reactive oxygen species: reaction mechanisms and relevance to Alzheimer's disease, Biochim. Biophys. Acta Protein Proteonomics 1703 (2005) 111–119, https://doi.org/10.1016/j.bbapap.2004.09.009.
[55] F. Leinisch, M. Mariotti, P. Hägglund, M.J. Davies, Structural and functional changes in RNAse A originating from tyrosine and histidine cross-linking and oxidation induced by singlet oxygen and peroxyl radicals, Free Radic. Biol. Med. 126 (2018) 73–86, https://doi.org/10.1016/J.FREERADBIOMED.2018.07.008.
[56] S. Vazquez, J.A. Aquilina, J.F. Jamie, M.M. Sheil, R.J.W. Truscott, Novel protein modification by kynurenine in human lenses, J. Biol. Chem. 277 (2002) 4867–4873, https://doi.org/10.1074/jbc.M107529200.
[57] N.R. Parker, J.F. Jamie, M.J. Davies, R.J.W. Truscott, Protein-bound kynurenine is a photosensitizer of oxidative damage, Free Radic. Biol. Med. 37 (2004) 1479–1489, https://doi.org/10.1016/j.freeradbiomed.2004.07.015.

[58] D.B. Medinas, F.C. Gozzo, L.F.A. Santos, A.H. Iglesias, O. Augusto, A ditryptophan cross-link is responsible for the covalent dimerization of human superoxide dismutase 1 during its bicarbonate-dependent peroxidase activity, Free Radic. Biol. Med. 49 (2010) 1046–1053, https://doi.org/10.1016/J.FREERADBIOMED.2010.06.018.

[59] M.S. Rogers, R. Hurtado-Guerrero, S.J. Firbank, M.A. Halcrow, D.M. Dooley, S.E.V. Phillips, P.F. Knowles, M.J. McPherson, Cross-link formation of the cysteine 228 − tyrosine 272 catalytic cofactor of galactose oxidase does not require dioxygen, Biochemistry 47 (2008) 10428–10439, https://doi.org/10.1021/bi8010835.

[60] E. Siakkou, M.T. Rutledge, S.M. Wilbanks, G.N.L. Jameson, Correlating crosslink formation with enzymatic activity in cysteine dioxygenase, Biochim. Biophys. Acta Protein Proteonomics 1814 (2011) 2003–2009, https://doi.org/10.1016/J.BBAPAP.2011.07.019.

[61] C.G. Davies, M. Fellner, E.P. Tchesnokov, S.M. Wilbanks, G.N.L. Jameson, The Cys-Tyr cross-link of cysteine dioxygenase changes the optimal pH of the reaction without a structural change, Biochemistry 53 (2014) 7961–7968, https://doi.org/10.1021/bi501277a.

[62] W. Li, E.J. Blaesi, M.D. Pecore, J.K. Crowell, B.S. Pierce, Second-sphere interactions between the C93–Y157 cross-link and the substrate-bound Fe site influence the O_2 coupling efficiency in mouse cysteine dioxygenase, Biochemistry 52 (2013) 9104–9119, https://doi.org/10.1021/bi4010232.

[63] R.J. Martinie, P.I. Godakumbura, E.G. Porter, A. Divakaran, B.J. Burkhart, J.T. Wertz, D.E. Benson, Identifying proteins that can form tyrosine-cysteine crosslinks, Metall 4 (2012) 1037, https://doi.org/10.1039/c2mt20093g.